A STUDY OF GIANT RADIO GALAXIES

A Thesis

Submitted for the Degree of

Doctor of Philosophy

in the Faculty of Science

By

LAKSHMI SARIPALLI

DEPARTMENT OF PHYSICS

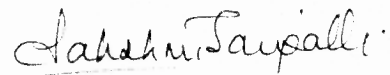**INDIAN INSTITUTE OF SCIENCE**

BANGALORE-560 012, (INDIA)

OCTOBER - 1988

DECLARATION

I hereby declare that the work presented in this thesis is entirely original, and has been carried out by me at the Tata Institute of Fundamental Research Centre, Bangalore, under the auspices of the Joint Astronomy Program of the Department of Physics, Indian Institute of Science. I further declare that this work has not formed the basis for the award of any degree, diploma, membership, associateship or similar title of any University or Institution.

Department of Physics
Indian Institute of Science
Bangalore 560 012
INDIA.

LAKSHMI SARIPALLI

ACKNOWLEDGEMENTS

It is a pleasure to thank my friends and colleagues Ravi Subrahmanyan, K. Indulekha, Ashok Singal, Tapasi Ghosh, Alok Patnaik, Sunita Nair and Vasudevamurthy for their friendship and help during my years here. They have provided me with moral support over difficult times ! My gratitude to all those friends at the Tata Institute of Fundamental Research Centre, Indian Institute of Science and the Raman Research Institute who made my stay here a pleasure. A special word of thanks to the TIFR Centre Library staff, in particular Ms. Meena Srinivasan, for providing a pleasant and affectionate atmosphere. I am grateful to Mrs. and Prof. A.K. Rao for their help and advice.

My thanks are due to Mr. R. Rajshekar of the Campus Electronic Impressions for the patient typing of my thesis; Ms. Shantha and Ms. Visalakshi of the TIFR Centre for their help in typing of parts of my thesis.

My parents, sisters and brother have always been a source of great encouragement to me. I am most grateful to them.

My husband, Ravi Subrahmanyan, has been a tremendous source of strength to me. Among innumerable other things, I thank him for his advice and guidance (scientific and non-scientific); for his understanding and patience.

CONTENTS

CHAPTER   I

INTRODUCTION AND SUMMARY

It is more than three decades since the discovery of the extended nature of radio galaxies. The pioneering radio interferometry of Cygnus A by Jennison and Das Gupta in 1952 established for the first time that radio emission associated with an active elliptical galaxy can arise mainly from a pair of lobes extending much beyond the optical extent of the galaxy, which is of the order of 10 kpc. Since then, studies of such powerful radio galaxies have revealed a plethora of fascinating though often intriguing structural details in them (Miley, 1980). Typically each of the two radio lobes possesses a bright emission peak ("hotspot") at its extremity, accompanied by a wake of diffuse emission ("tail") extending towards the parent galaxy from each side. Most of the models proposed for explaining these structures, although agree in the location of the energy source, differ in the nature of the transport of energy to the outer regions. The plasmon models (De Young and Axford, 1967; Christiansen et al., 1977) require the energy supply to be in the form of discrete plasmons of relativistic particles and magnetic field ejected from the galactic nucleus. The beam models on the other hand require the energy supply to be a more-or-less continuous flow of relativistic particles and magnetic field (Rees, 1971; Blandford and Rees, 1974; Wiita, 1985; Bridle, 1987). Radio observations with improved resolution and sensitivity and the modern image reconstruction techniques

have over the years provided direct support for the continuous beam models via the discovery of jets seen connecting the parent galaxy and the hotspots and the disk-like structures seen in some well-resolved hotspots.

An important new dimension was added with the discovery of two double radio galaxies in which the radio lobes were found to be separated by megaparsecs, which exceeds the typical sizes of radio galaxies by more than an order of magnitude (Willis, Strom and Wilson, 1974). The lobe separation of 5.7 Mpc measured for one of these two 'giant radio galaxies' (GRGs), namely 3C236, makes it the largest radio galaxy known to date. Radio galaxies of such exceptionally large sizes have only been found at small redshifts (z < 0.25) where they constitute a small fraction (<5%) of all powerful radio galaxies. Double radio sources at the other extreme in physical size are the so called "compact doubles" (CDs), in which the lobes are yet to emerge out of the innermost 1 kpc of the parent elliptical galaxy (Phillips and Mutel, 1980; Hodges and Mutel, 1986). Both GRGs and CDs exhibit morphologies basically similar to that observed in radio galaxies of typical size ($\sim 10^2$ kpc).

Despite the success of the continuous beam models, little is understood of the process of radio galaxy evolution. Although, it seems increasingly clear that despite the enormous range in physical size, the CDs, normal-size double radio sources and GRGs are manifestations of the same

basic phenomenon, it is not clear if they necessarily form an evolutionary sequence. A directly related question : what causes the exceptional sizes of the GRGs? -forms the major theme in this thesis. Although somewhat older than normal size sources (Fig.2.7, Chapter II), GRGs are far from being 'relic' radio galaxies of the type considered by Goss et al.(1987), Cordey (1987), Giovannini et al. (1988). Unlike such sources GRG possess integrated spectra typical of the general population of the radio galaxies and even possess bright hotspots in some cases (Tsien, 1982; Chapter III). Radio jets and cores are frequently detected in them (Chapter IV), again indicative of continuing activity of the central engine of the parent galaxy. Existing optical data reveal their parent galaxies to be typical (see Chapter IV) and as discussed in Chapter V, their environments are probably not significantly different from those of typical 'edge-brightened' radio soruces.

In this thesis we focus attention on a sample of 15 GRGs consisting of all 15 published cases where the radio source size is known to clearly exceed 1.5 Mpc (taking a Hubble constant of H_0 = 50 $kms^{-1}Mpc^{-1}$, in order to be consistent with most of the literature on GRGs). This defining criterion corresponds to 1 Mpc for H_0 = 75 $kms^{-1}Mpc^{-1}$ which is more commonly used these days. Our sample of GRGs consists of 1 quasar and 14 radio galaxies, including 0503-286 discovered by us at Ooty, whose size of 2.5 Mpc makes it the largest known radio galaxy in the southern hemisphere. We

present radio as well as detailed optical spectroscopic observations of this object. For another 4 GRGs in the sample we have augmented the radio data with fresh observations made the Very Large Array (VLA). Large-scale optical fields around 7 of the GRGs were quantitatively examined, with the objective of studying the galaxy environment around GRGs and its relation to their radio structure. This study is facilitated by the fact that all 15 GRGs are relatively nearby objects with $z < 0.1$ in 11 cases and $z < 0.25$ in all 15 cases. The source HB13 originally discovered in the 6C survey, which is a striking example of twin-jet morphology (Masson, 1979), has not been included for the present in the GRG sample, because its connection with the large diffuse radio emission, suspected from the 6 C map, is not obvious from the recent WSRT observations at 610 MHz (Jägers, 1986).

The GRGs exhibit a variety of structural types including the edge-brightened (FRII; Fanaroff and Riley, 1974) structures, edge-darkened (FRI), twin-jet, and inversion symmetric structures (Z-shaped). Among individual GRGs, we commonly find examples of mixed morphology, where one radio lobe is edge-brightened while the other is not (DA240, 4C73.08, 3C326, NGC6251). This behaviour is not entirely consistent with the simple classification scheme of Fanaroff and Riley (1974), although it can be attributed to the radio luminosities of GRGs being close to the transition between the two morphological classes (Chapter II). Some of

the specific advantages offered by GRGs include:

(i)   The large angular sizes (>10') permit exceptionally detailed mapping of the brighter features, such as the jets and hot spots.

(ii) Inverse Compton scattering of the microwave background photons being usually the dominant energy loss process for the relativistic electrons inside the lobes of GRGs, their ages estimated from spectral gradients are much less affected by the poor knowledge of the history of magnetic field inside the lobes (Chapter II).

(iii) The extremely large projected size being the defining criterion for GRGs, their main axes are expected to be inclined away from the line-of-sight. Hence, the observed emission from their cores, jets, hotspots and other parts is expected to be much less affected by projection effects.

(iv) Since the radio lobes of GRGs, have already penetrated well beyond the interstellar medium (ISM) of the parent galaxy and are presumably interacting directly with the intergalactic medium (IGM), GRGs can serve as unique probes of the IGM.

Further, as pointed out by Baldwin (1982), the frequency of occurrence of GRGs in a complete sample of radio sources can place strong constraints on the evolution of radio luminosity (P) with the growing size (D). This and the first two of the above points have been systematically exploited, notably by Saunders (1982) and Saunders et al.

(1981). In the present dissertation, an attempt is made to pursue all these aspects. Additionally, we investigate the properties of the radio cores, hot spots and the environments surrounding GRGs, from both observational and theoretical considerations. Briefly, the contents of the various chapters are as follows :-

Chapter II: This Chapter presents the discovery of the GRG 0503-286 with the Ooty Synthesis Radio Telescope (OSRT) and the extensive follow-up radio observations with the Effelsberg and VLA telescopes, supplemented by sensitive, high-resolution optical spectroscopy at La Silla. With an overall size of 2.5 Mpc, this is the largest known radio galaxy in the southern hemisphere. From the observed gradients of radio spectral index we infer an age of $\sim 10^8$ years. The radio morphology of this double source is highly asymmetric, which is discussed in terms of the observed asymmetry of the galaxy distribution in the field of this source. Located at z = 0.038, this GRG is exceptional in being a member of what looks like a cluster rich enough to belong to Abell class 0 or higher.

Chapter III: We have tried to deduce the run of minimum pressure, P_{min}, along the axes of the radio lobes which are expected to be directly interacting with the IGM. The lower envelope of the derived values of P_{min} seem to be rather well defined and occurs at a value of $\sim 2.10^{-14}$ dyn.cm^{-2} which amounts to a reliable upper limit to the IGM pressure, provided the minimum energy condition applies to the relaxed

lobes. Constraints on the collimation of beams in double radio sources upto megaparsecs from the nucleus are derived from an analysis of the observed hot spots in the GRGs and in a carefully selected comparison sample of 15 normal size radio galaxies. The study rules out the possibility of narrow beam opening angles as the cause for the exceptionally large sizes of GRGs. This analysis also shows that the beams powering the GRGs are intrinsically as energetic as those sustaining the order-of-magnitude more lumunious radio galaxies of normal size.

Chapter IV: Radio detections of the nuclei are now available for all radio galaxies in the GRG sample, excepting the two southern GRGs whose published maps suffer from limited dynamic range. The prominence of the cores (=core flux/total flux) of the GRGs is statistically compared with that deduced for a well-defined comparision sample comprising of 35 radio galaxies of normal dimensions but matching the GRGs in the range of radio luminosity and redshift. It is interesting that the cores in GRGs are found to be at least as prominent as those in the much smaller comparison sources, despite their presumably younger evolutionary stage as well as the higher probability of relativistic beaming of the core emission expected for the comparison sources with smaller projected size. The intrinsically high prominence of the cores of GRGs, despite their being highly evolved radio sources seems to offer a useful clue for understanding the origin of such large radio structures.

Chapter V: The Chapter presents a quantitative study of the environments around 7 GRGs for which sufficiently deep, wide-field optical plates are available. For each case, a $2^{\circ}\times2^{\circ}$ field roughly centred at the GRG was digitized using the COSMOS measuring machine (Edinburgh) and a cross correlation analysis of the galaxy clustering around the GRGs was carried out following the basic technique described by Longair and Seldner (1979). This study shows that, on an average, GRGs lie in as sparse regions as the powerful, edge-brightened radio galaxies. We further find that in 5 of the total 6 GRGs which show an appreciable asymmetry in lobe separation from the nucleus, the galaxy clustering is clearly higher on the side of that radio lobe which lies nearer to the nucleus. This correlation strengthens the prospects of being able to infer the ambient gas density from the observed distribution of galaxies around a given location in even sparsely populated regions of space.

Chapter VI: This chapter presents an attempt to predict the numbers and mean radio luminosities of GRGs in successive bins of redshift upto z = 0.6, adopting a realistic sensitivity limit of 1 Jy at 1 GHz for any dedicated search programme plausible in future. These estimates are based on a model for the beam propagataion first through the hot gaseous halo around the parent galaxy and thereafter through the even hotter but less dense IGM. The model has been generalized to allow for any relativistic motion of the hotspots as well as for the expected reduction in the radio output due to

enhanced inverse Compton losses against the Microwave Background photons within the expanded radio lobes. Taking the observationally determined values for the key parameters of the beams, galaxy haloes and IGM and assuming a reasonable value of the order of 10^8yr for the duration of nuclear activity, the model is able to successfully reproduce the observed numbers and mean radio luminosity of GRGs at small redshifts ($z < 0.1$). Further, it predicts that a comparable number of GRGs should be found at higher redshifts ($z>0.1$) by a concerted high-resolution follow up of the existing surveys like the 6C survey (Baldwin et al., 1985).

Chapter VII: With an overall size of >1/2 Mpc the nearest radio galaxy, Centaurus A is not only a kin to GRGs but also a testbench for investigating the radio galaxy phenomenon. The availability of wide-field radio and optical images for this object has enabled us to discover interesting spatial coincidences between the radio and optical features in the source. Based on this, a new interpretation is proposed for the inversion symmetric, multi-peaked radio morphology of this source, which does not require the central engine to precess. Further, to explain the bending and flaring of the radio jet a new mechanism is proposed, based on the apparent interception of the jet by a (rotating) shell segment, probably a relic of a disk galaxy captured by Cen A, $\sim 10^9$ years ago. This interpretation permits us to estimate the gas density within the shell ($>10^{-27}$gm.cm^{-3}) and also yields a new method for estimating the magnetic field strength inside

the northern inner radio lobe seemingly created in the aftermath of the jet-shell collision. The field of 18μG, thus estimated, is close to the value of 14μG deduced from the minimum pressure argument.

Chapter VIII: In this chapter useful constraints are placed on some physical parameters of classical double radio sources, using a sample of 10 bright hot spots associated with such sources and employing the beam model. Constraints are thus placed on densities, bulk velocities, mass-flow rates and radio efficiencies of the beams. It is further shown that the outflow velocity of the relativistic electrons present inside the hotspots increases with the beam velocity and attains a maximum value of 0.25c. Continuing the same approach and assuming that the usual equipartition condition prevails inside the hot spots, assumed to be roughly spherical in shape, we arrive at an explanation for the well known trend that the hot spots found in sources of lower luminosities are generally more diffuse. It is further argued, that non-relativistic beam velocities (<0.1c) can only give rise to hot spots of luminosities upto $\sim 10^{44}$erg s^{-1}. For hot spots powered by relativistic beams, much higher luminosities are atainable but a qualitative change in morphology should occur above a luminosity of $\sim 10^{46}$ erg s^{-1}.

CHAPTER II

A NEW GIANT RADIO GALAXY 0503 - 286

2.1 INTRODUCTION

The several special attributes of giant radio galaxies (GRGs), as outlined in Chapter I, make them interesting objects for study. It has been recognized (Willis et al., 1974; Mayer, 1979; Saunders, 1982) that their large sizes and ages can be useful for constraining the physical processes believed to be operating in radio galaxies, like energy replenishment mechanisms, acceleration processes, confinement etc. GRGs provide high relative linear resolutions at any given redshift and they could be used as probes of the Intergalactic Medium (IGM). Further, since most GRGs are likely to lie in the plane of the sky they enable studies of intrinsic parameters, largely free of projection effects (Saripalli et al., 1986; Saripalli and Gopal-Krishna, 1987). The statistical nature of many such studies demands a fairly large sample of GRGs. There have been several searches for large radio sources (e.g., Willis et al., 1974; Waggett et al., 1977; Masson, 1979; Mayer, 1979; Faulkner, 1986; Saunders et al., 1987). The strategy followed by the Westerbork group was to map candidate GRGs selected from the pencil-beam survey of Bridle et al., (1972) at 1.4 GHz, with high sensitivity, dynamic range and arc-minute resolution, using the WSRT. 3C 236, DA240, NGC315 and 3C326 were established as GRGs by this approach. The Cambridge group followed up the cases of structures with low surface

brightness, detected with the 6C synthesis telescope. This method yielded 4 new, confirmed GRGs: 4C39.04, 4C40.08, 4C73.08 and NGC6251. While all these efforts were confined to the northern quarter of the celestial hemisphere, no comparable search for GRGs has been reported for the southern skies, though a program using MOST is in progress (W.B. McAdam, personal communication).

Recognizing the need to extend such searches to the lower declinations, we planned a systematic search for GRGs using the Ooty Synthesis Radio Telescope (OSRT),concentrating largely on the southern sky. The method of search together with a brief description of the OSRT is given in the next section, followed by the details of the GRG 0503-286 discovered by us.

2.2 THE TELESCOPE

The OSRT (Swarup, 1985) operates on the principle of 'earth-rotation aperture synthesis'. The array consists of 7 small cylindrical antennas (size : 9m x 23m) used in conjunction with the large Ooty radio telescope (ORT; Swarup et al., 1971) that has been electrically subdivided into 5 sections (each of size : 30m x 92m). All the 12 elements are parabolic cylinders oriented in the N-S direction along a slope equal to the geographic latitude of the station (ϕ = $+11^{\circ}22'$). Each of these elements is mechanically steerable in the E-W direction. Steering in the N-S direction is done by electrically phasing the dipole array and allows a coverage of $\pm40^{\circ}$ in declination. The field of view of the OSRT has a

HPBW of $3^{\rm O}$ (E-W) x $0^{\rm O}.7$(N-S) using only baselines involving one of the ORT sections and one smaller cylinder. The N-S field of view can be widened by using only half of each of the ORT modules (=48 dipoles) in each of the 5 ORT sections. The smallest synthesized beam width is $0'.6$ x $0'.9$ (HPBW) after a full 9-hour tracking, which gives an rms sensitivity of $\sim$5 mJy/beam. With the existing 2-bit digital correlator, it is possible to intercorrelate signals between antenna pairs over all the 66 baselines available. However for the observations described here we used only the correlations of each of the 7 antennas with the 5 sections of the ORT (35 baselines). This was because of low sensitivity on the baselines involving the 7 smaller antennas and also in order to avoid problems arising from different baselines having differing fields of view.

2.3 THE SEARCH PROCEDURE FOR GRG CANDIDATES

We define a giant radio galaxy as having a largest linear size (measured between the outermost 3σ contours) of >1.5 Mpc (H_O = 50 kms^{-1}Mpc^{-1} and q_O = 0). We adopted the following search procedure for them: pairs of radio sources listed in Molonglo Reference Catalogue (Large et al., 1981) in the declination range of $-30^{\rm O}$ to $+18^{\rm O}$ were selected, which satisfied the following criteria: (a) an angular separation between the pairs in the range 15' to 45', and (b) atleast one member constituting the pair listed as 'extended' (ie., > 1') or as 'complex'. The separation criterion is expected to optimise the search for GRGs over the easily identifiable

magnitude range for the parent galaxy ($m_R \lesssim 17$). In addition, restriction to relatively bright magnitudes reduces the probability of the suspected optical counterpart turning out to be an unrelated background object (since counts increase sharply at fainter magnitudes). The second criterion of altleast one member of the pair being resolved goes to increase the possibility of their being associated and not being merely cases of chance projection since individual lobes in known GRGs are large, well resolved features. Optical field of each of the selected pairs (numbering ~ 200) was examined on the Palomar Sky Survey (PSS) prints. We selected only those pairs where a bright elliptical galaxy ($m_R < 17$ mag) was seen located roughly midway between the radio source pair, but not coinciding with either member of the pair. We selected 12 pairs as the first set of candidates for radio imaging with the objective of detecting any diffuse bridge of emission connecting the pair, thereby confirming their association. In the following section we describe observations of one such pair listed as 0503-284 and 0503-290 in the Molonglo Catalogue, which we have confirmed as a GRG.

2.4 RADIO OBSERVATIONS

Table 2.1 summarizes the radio observations of this source. The result of these observations are presented in the form of contour maps in Fig.2.1-2.2. The OSRT observations at 327 MHz (Fig.2.1a-b) were made after widening the field of view as discussed earlier. The resulting primary beam was $\sim 3^{\circ}$ (RA) x $1^{\circ}.3$ (DEC). The scatter of the measured visibility
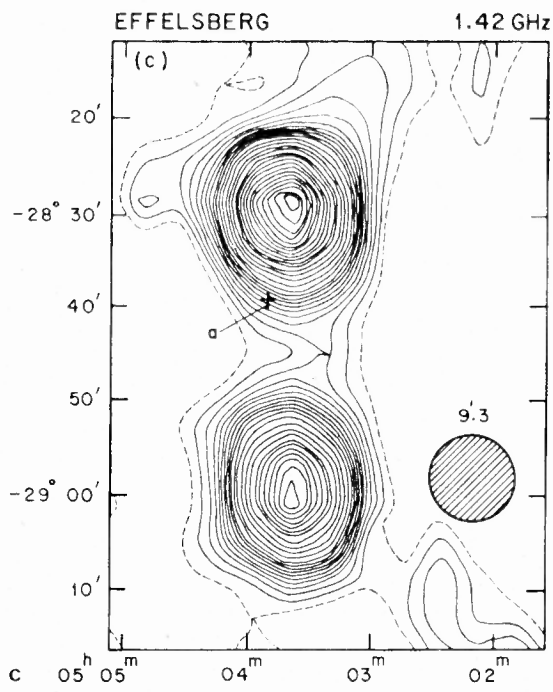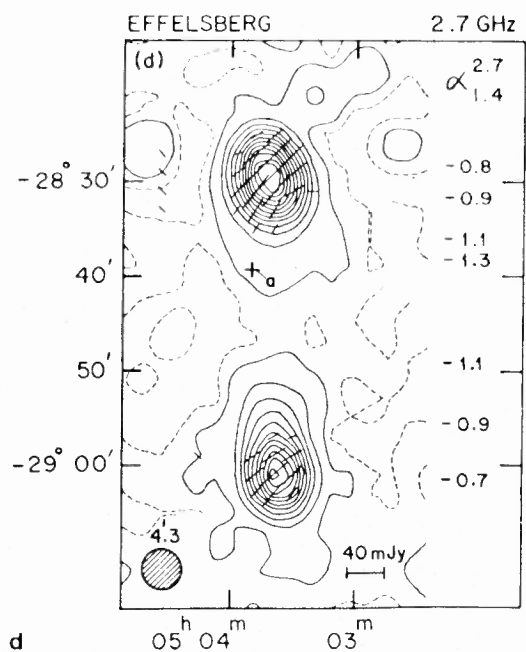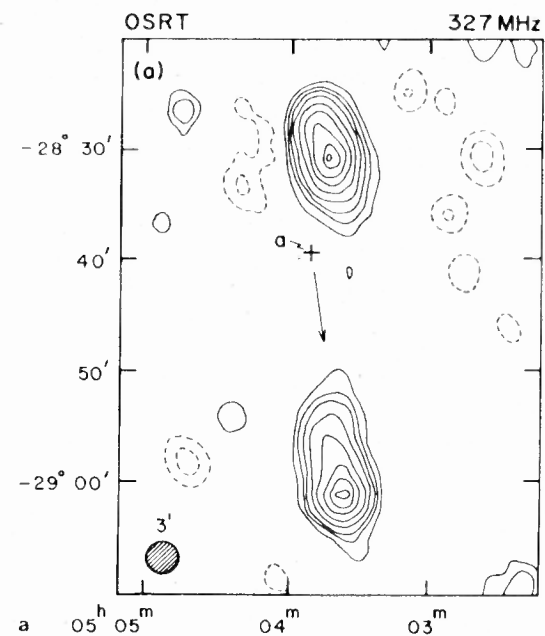
Table 2.1. Summary of the Observations:

Freq (MHz)	Telescope	Beamwidth (HPBW)	Calibrator	Flux Jy	Reference
327	OSRT	1'.5 x 1'.5 3' x 3'	0519 − 208	8.5	Saripalli et al., (1986)
1420	Effelsberg	9'.3	3C71	5.1	" "
2695	Effelsberg	4'.3	3C286	10.4	" "
1465	VLA	15" x 15"	0451−282	2.4	Saripalli et al., (1988)
4885	VLA	4" x 4"	0451−282	1.9	" "

Table 2.2 The observed optical absorption and emission lines from the galaxies 'a' and 'b'

	Line	Observed $\lambda_{peak}[\text{Å}]$	Redshift	Relative flux
Galaxy 'a'	Mg$\,$I $\lambda 5173$	5370.2	0.0381	abs.
	Na$\,$I $\lambda 5893$	6116.7	0.0380	abs.
	[O$\,$I] $\lambda 6300$	6527.5	0.0361	59
	Hα + [N$\,$II] $\lambda 6583$	6827.3	0.0387	100
	[S$\,$II] $\lambda 6717, 6731$	6976.5	0.0376	31
			$\langle 0.038 \pm 0.001 \rangle$	
Galaxy 'b'	Mg$\,$I $\lambda 5173$	5372.9	0.0386	abs.
	Na$\,$I $\lambda 5893$	6117.6	0.0381	abs.
			$\langle 0.038 \pm 0.001 \rangle$	

OSRT   **327 MHz**

(b)

-28° 25′

-28° 45′

-29° 05′

1.5

b   05ᵐ   04ᵐ   05ʰ 03ᵐ

OSRT   **327 MHz**

(a)

-28° 30′

40′

50′

-29° 00′

3′

a   05ʰ05ᵐ   04ᵐ   03ᵐ

Fig.2.1a Total intensity distribution of 0503-286. The shaded circle represents the restoring beam used. The '+' sign marks the position of the parent galaxy 'a', (a) 327 MHz, OSRT map made with a beam of FWHM 3' x 3'arc. Contours are drawn at (-1, -0.5, 0.5, 1, 1.5, 2.5, 4, 6, 8, 10, 11) x 107 mJy per beam. (b) 327 MHz, OSRT map made with the beam of FWHM 1'.5 x 1'.5 arc. Contours are drawn at (-0.5, -0.25, 0.25, 0.5, 1, 1.5, 2, 2.5, 3, 3.5) x 107 mJy per beam. The dots represent neighbouring galaxies within ±2 mag of the magnitude of 'a'; 'b' is a spiral galaxy with a redshift same as that of 'a' (Section 2.4). (c) 1.4 GHz map made with the 100 m Effelsberg dish, with a beam of FWHM 9'.3 x 9'.3 arc. Contours are at 25 mJy for the first 10 contours, and 50 mJy thereafter. (d) 2.7 GHz map made with the Effelsberg dish with a beam of FWHM 4'.3 x 4'.3 arc. Contours are drawn at intervals of 29 mJy/beam. The lines represent E vectors, with their magnitudes proportional to the linearly polarized flux, as defined by the horizontal bar. The vertical array of numbers represent the run of spectral index along the source axis, nearly coinciding with the north-south line drawn through ∝ = 05ʰ03ᵐ39ˢ.

EFFELSBERG   **2.7 GHz**

(d)

∝ 2.7 / 1.4

-0.8
-0.9
-1.1
-1.3

-28° 30′

40′

-1.1

50′

-0.9

-29° 00′

-0.7

4.3

40 mJy

d   05ʰ 04ᵐ   03ᵐ

EFFELSBERG   **1.42 GHz**

(c)

20′

-28° 30′

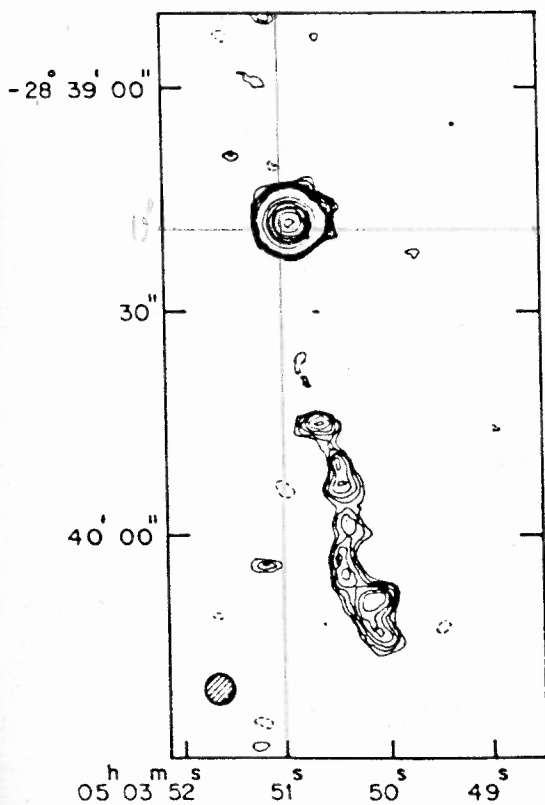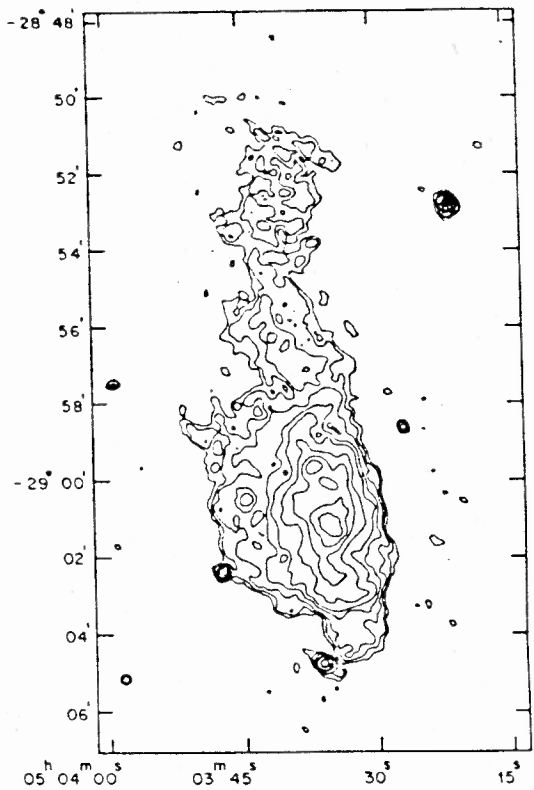40′

a

50′

-29° 00′

9.3

10′

c   05ʰ05ᵐ   04ᵐ   03ᵐ   02ᵐ
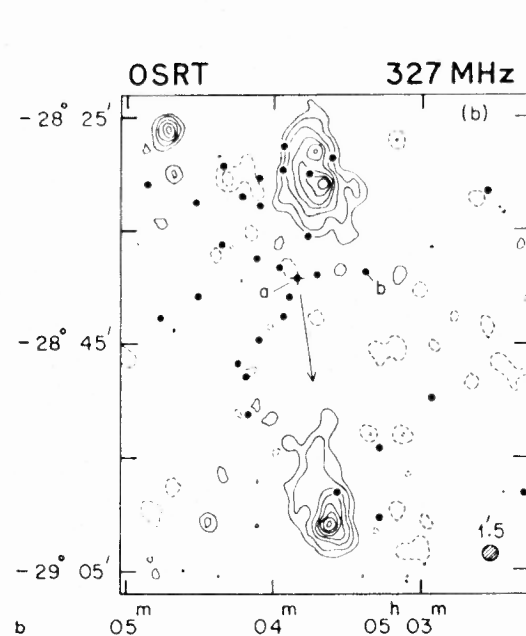
Fig.2.2(a) Total intensity distribution of the northern lobe of 0503-286 observed with the VLA at 1.4 GHz, using a restoring beam of FWHM 15" x 15" arc. The core and jet structure are seen towards the south. Contours are drawn at -0.6, 0.6, 1, 1.5, 2, 3, 4, 5, 7, 10, 15, 20, 25, 30, 35, 40, 45, 50, 55, 60, 65, 70, 75 mJy/beam; (b) Same as (a) for the southern lobe. Contours are drawn at -0.5, 0.5, 0.7, 1, 1.5, 2, 3, 4, 5, 6, 8, 10, 12, 14, 16, 20, 25 mJy/beam;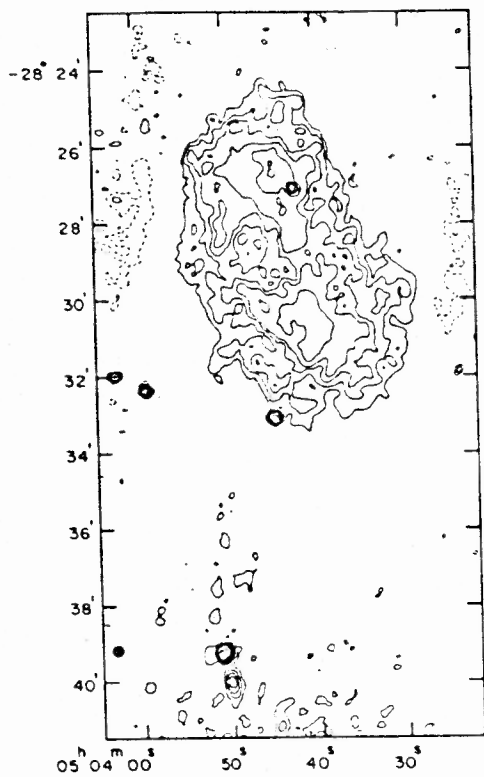 (c) Total intensity distribution of the core and jet of 0503-286, observed with the VLA at 5 GHz, using a restoring beam of FWHM 4"x4" arc. Contours are at -0.15, 0.15, 0.175, 0.2, 0.225, 0.25, 0.28, 0.32, 0.36, 0.4, 1.0, 1.5, 2, 2.5, 3, 4, 5 mJy/beam.

points peaked around 9 Jy. Since the shortest available spacing in the north-south direction is 90λ, structures on scale >15' in declination are likely to be poorly represented in the data. For the 327 MHz maps shown in Fig.2.1a-b the contour values have been corrected for the attenuation caused by the OSRT primary beam.

The maps shown in Fig.2.1c-d at 1.4 and 2.7 GHz, respectively, were obtained with the 100m dish at Effelsberg (Bonn). The reduction of the data was done using the NOD2 map making procedure (Haslam, 1974).

As a follow-up of these initial observations, we mapped with the VLA the lobes at 1.4 GHz and just the core region at 5 GHz. The large angular size necessiated separate observations of the northern and southern lobes (Field centers: $05^h03^m45^s-28^\circ33'00"$ and $05^h03^m38^s-28^\circ58'00"$ respectively) These 1.4 GHz observations were made in the B/C hybrid array configuration, while the 5 GHz observations (centred at the position of the optical galaxy) were made in the A/B hybrid configuration. Flux density of the secondary calibrator 0451-282 (Table 2.1), was boot-strapped to the flux densities of the primary calibrators, 3C138 and 3C48. Analysis of the data was done at Ooty using the NRAO AIPS routines on a VAX 11/750. The maps are shown in Fig.2.2(a-c) after applying a correction for the attenuation caused by the finite primary beamwidth.

2.4. OPTICAL OBSERVATIONS

On examining the optical fields of the source on the PSS prints, we identified the 15-mag elliptical galaxy located at "a" (Fig.2.1) as the parent galaxy. This identification was suggested because (1) it was seen located between the two radio lobes, close to the line joining them and because it was clearly the brightest among the galaxies seen between the lobes and (2) it appeared to be the dominant member in a group of galaxies (Section 2.5). This circumstance would make it an almost exclusive candidate for strong radio emission (see Menon and Hickson, 1985) The galaxy is centred at the following position with an uncertainty of 2 arc sec in each coordinate

$$\alpha \, (1950) = 05^h 03^m 51.0^s \quad \delta(1950) = -28^{\circ}39'19"$$

Optical spectroscopic observations of this elliptical galaxy were carried out using the 2.2 metre telescope of the Max-Plank Institut fur Astronomie, at La Silla, during the dark night of March 14, 1985. The CCD spectrograph used was equipped with a RCA chip of 512 x 320 pixels detecting the spectrum between effective wavelengths of 4800 A and 8000 A. Two spectra with integration times of $\sim$ 15min each were taken through a long slit with a low spectral resolution of 13 Å. The standard reduction of the spectrum involved dividing the CCD frames by a flat field, extracting the spectrum and sky background, correcting for galactic extinction, and flux calibration by comparison with standard stars. The resulting spectrum shows a superposition of a

featureless red continuum, an absorption-line galaxy spectrum and an emission line spectrum (Fig.2.3a). The relatively strong and narrow emission lines of (OI) (λ 6300), Hα and [SII] ($\lambda\lambda$ 6717,6731) were seen, providing evidence for nuclear activity. Hβ emission was not detected, possibly indicating strong internal reddening by dust. Strong absorption features of MgI ($\lambda\lambda$5167,5173,5184) and NaI ($\lambda\lambda$5890,5896) seen in the spectra are signatures of the underlying galaxy. We also carried out on this occasion similar spectroscopic observations of another bright galaxy ($\sim$16-mag) marked as 'b' in Fig.2.1b. It is a spiral. The absorption features of MgI and NaI detected in its spectrum are, within the errors, identical in redshift to that of the radio galaxy 'a' (Fig.2.3b). Since the absorption line spectra of the two underlying galaxies are similar we have normalized and subtracted the fainter from the brighter one, in order to reduce the effect of absorption features on the emission line strengths (Fig.2.3c). The three emission lines mentioned above are clearly visible; the slope in the differential spectrum is probably due to a featureless red continuum from the galaxy 'a', frequently seen in active galactic nuclei, rather than indicative of calibration problems. In Table 2.2 we list the observed wavelengths of identified absorption and emission line features along with their derived redshifts. The relative line strengths of the emission lines are also given; these were derived from the differential spectrum (Fig.2.3c). The observed mean redshift

galaxy 'a'

MgI   NaI   B-band
A-band

galaxy 'b'
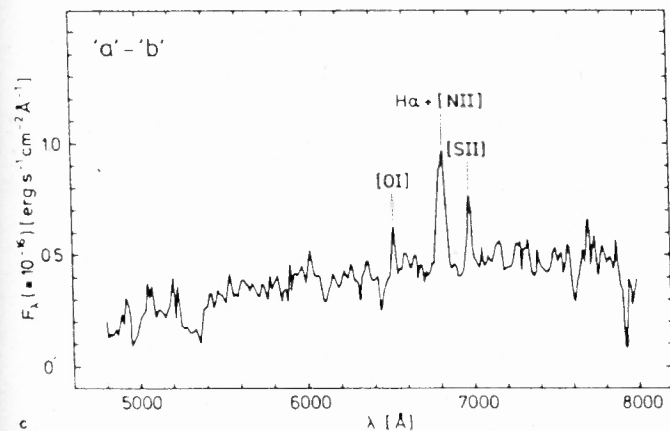

'a'-'b'

Hα+[NII]
[SII]
[OI]
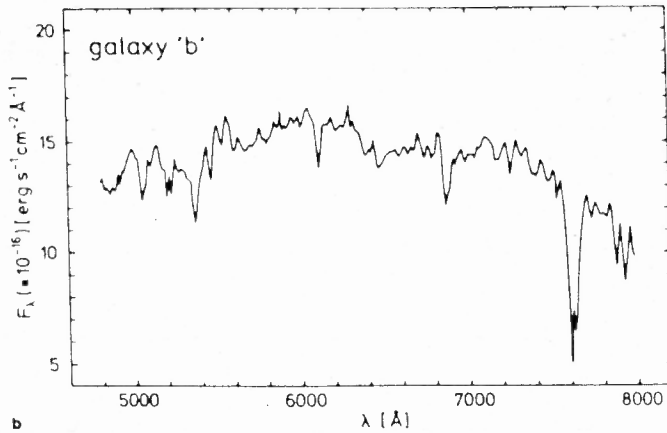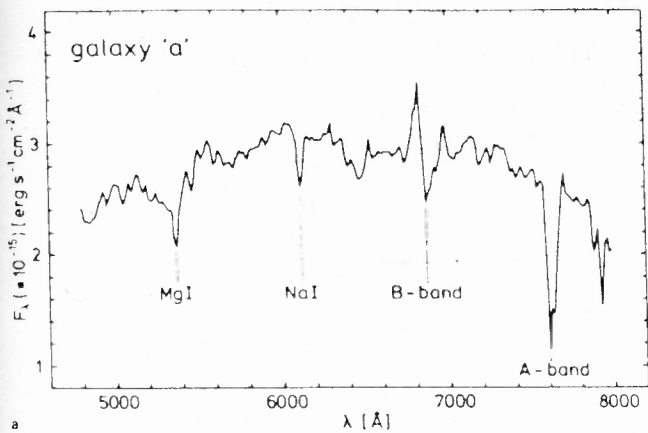
Fig.2.3(a)   Optical low dispersion spectrum of galaxy 'a';
besides the atmospheric A- and B-bands strong absorption
features of redshifted MgI and NaI are detected, as well as
three emission lines; (b) same as in (a) for galaxy 'b' but
no trace of any emission lines; (c) the difference spectrum,
'a'-'b', after normalizing spectrum of 'b' at 6650 Å to the
flux density level of 'a'. The underlying red continuum and
emission lines in galaxy 'a' are apparent.
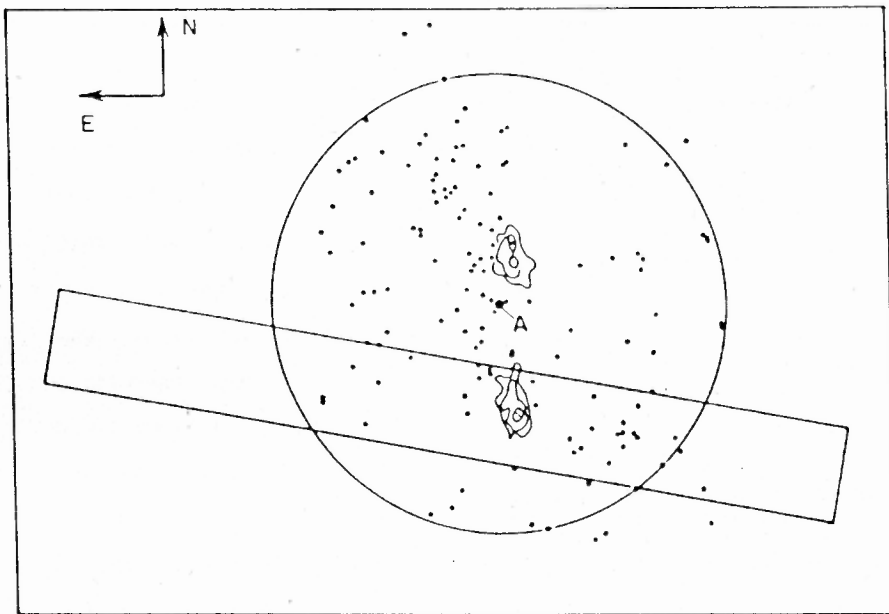
Fig.2.4   The optical field of 0503-286, with the 1'.5 arc,
327 MHz OSRT map superimposed. The parent galaxy is marked as
'a'. The circle corresponds to a radius of ~ 3 Mpc. Dots
represent the neighbouring galaxies with (eye-estimated) red
magnitudes within ±2 of the magnitude of 'a'. The rectangular
box is the HEAO A-1 error box.

Table 2.3 Observed Parameters of 0503-286

Optical Position $= 05^h\ 03^m\ 51^s.0\ -\ 28^{\circ}\ 39'\ 19''\ (\pm 2'')$

Redshift z $= 0.038 \pm 0.001$

Distance (Mpc) $= 216$

LAS (') $= 40$

LLS (Mpc) $= 2.5$

PA ($^{\circ}$) $= 2$

	Integrated	North lobe	South lobe	Core	Jet
$S_{1.4}$ (Jy) (HPBW)	2.8 (9'.1)	1.6 ± 0.15 (9'.1)	1.2 ± 0.1(9'.1)	0.021 (15''.)	0.0085 (15'')
$S_{2.7}$ (Jy) (HPBW)	1.62 (4'.3)	0.85 ± 0.05 (4'.3)	0.77 ± 0.05(4'.3)	-	
S_5 (Jy) (HPBW)	-	-	-	0.0064 (4'')	0.003 (4'')
$P_{1.4}$ (WHz^{-1})	$1.8.10^{25}$	$1.0.10^{25}$	$7.7.10^{24}$	$1.3.10^{23}$	$5.4.10^{22}$
Spectral index (α)	1.06 ± 0.06	1.0 ± 0.2	0.7 ± 0.2	0.26	0.5
% Polarisation at 2.7 GHz(Total)	-	12	6.5	-	-
% Polarization at 2.7GHz (Peak)	-	17	7.8	-	-

* $S_\nu \propto \nu^{-\alpha}$

Table 2.4 Derived Parameters

	North	South
Lobe size (Kpc x Kpc)	582 x 332	1337 x 323
Max. core-lobe Separation (Kpc)	965	1721
Lobe axial ratio	1.75	4.14
Asymmetry factor (D)	1.9	
Lobe Misalignment (deg)	16	~0
Length of jet (Kpc)	43	
Emission gap (Kpc)	12.7	
Core fraction (%) at 5GHz	0.71	
Lobe energy density (erg cm^{-3})*	$5.9.10^{-14}$ at a sep.of 450 Kpc from core	$5.4.10^{-14}$ at a sep.of 850 Kpc from core.
Hotspot energy density (erg cm^{-3})*	-	$3.3.10^{-13}$
Lobe Magnetic field (μG)	0.9	0.8
Lobe spectral age (yr)	$4.5.10^7$	$7.1.10^7$
Average hotspot speed	0.07c	0.08c

*Assuming equal energy density between relativistic electrons and protons, and a filling-factor of unity.

of both galaxies is Z = 0.038 $\pm$ 0.001.   These two galaxies
and possibly several others seen in their vicinity may thus
be members of a group or cluster of galaxies that seems to be
stretched mainly along the northern and eastern edges of the
radio galaxy (Fig.2.1b, Fig.2.4). As the source lies at the
edge of the PSS plate, it was not possible to include it in
our sample of GRGs for which we obtained a scan of the
optical fields using the COSMOS machine (see Chapter V).
Nonetheless, we have examined the field over a region of 2° x
2° centred on the parent galaxy "a".   A portion of it is
shown in Fig.2.4, where all galaxies within 2 mag of that of
the parent galaxy 'a' are marked (we hope this way to
minimise the cases of chance projection). Also indicated is
the HEAO - A1 error box for X-ray emission (Wood et al.,
1984), which is centred close to the weaker southern radio
lobe.

2.5 RESULTS

In Table 2.3, we list the observed source parameters,
and in Table 2.4, the derived parameters. We measure an
angular size of $\sim$ 40.3 between the outermost (3σ) contours
on our 1.4 GHz VLA map (Fig.2.2).   At the measured redshift
of 0.038, this corresponds to a linear size for the source of
$\sim$2.5 Mpc, making it the largest radio galaxy known so far in
the southern hemisphere.   The power of this source is
$\sim 1.8.10^{25}$ WHz^{-1} at 1.4 GHz which is close to the value that
roughly separates edge-brightened (FRII class) from edge-
darkened (FRI class) radio galaxies. From Fig.2.1 and 2.2 it

is seen that the source does not possess any "compact hotspots" but has only "warmspots" in its lobes. Our VLA observations reveal an unresolved component (< 4") at the position of the galaxy "a", and a clearly visible wiggly jet pointing at the southern lobe. No counter-jet is seen in our maps. Much of the emission in this source comes from diffuse regions which are missed out in our synthesis maps because of their very low surface brightness, and the lack of short UV spacings in the data (minimum spacing=350λ). The northern lobe has two peaks of emission, and the whole lobe is disoriented by an angle of 17° from the line joining the core to the outer peak (Fig.2.2a). The southern lobe on the other hand shows only one prominent peak and a tail of emission extending along the line joining the peak to the core. The core itself is seen to be misaligned from the radio source axis by a large angle, $\sim$ 16° (defined as the supplement of the angle subtended at the core by the outermost peaks). The peak in the southern lobe, too, is clearly recessed from the lobe's edge. But, the northern and southern lobes are, otherwise, seen to be very dissimilar in appearance. Many point sources are seen in the field of this source and they are most likely to be background sources including the one at α =05^{h}03^{m}36.3^s, δ = 29°04'46.9" (Fig.2.2b) . In Fig.2.4 we show the optical environment of the GRG within a radius of $\sim$ 3Mpc. The neighbouring galaxies plotted as dots are all within 2 magnitudes of that of the parent galaxy 'a', based on our eye estimates using the PSS prints. They reveal a remarkable concentration of the galaxies to the north-east of

the GRG. The counts of galaxies within the 3 Mpc radius circle could easily classify the 'clustering', on the Abell richness scale O or higher.

In Fig.2.5 a plot of the integrated spectrum of the source is given. The flux densities are on the scale of Baars et al. (1977). The integrated spectral index is found to be +1.06 ($S_{\nu} \propto \nu^{-\alpha}$). Fig.2.6 shows a contour plot of the spectral index between frequencies 1.4 GHz and 2.7 GHz using the single dish (Effelsberg) maps. A clear steepening of the spectrum is seen from the outer to the inner regions in each lobe. Such a pattern of spectral gradient is known to characterise lobes of many powerful, extended double radio sources (eg., Miley, 1980). It is indicative of synchro Compton aging of the relativistic electrons left behind by the advancing hotspots. Using injection spectral indices of α = 0.6 and α = 0.7, at the northern (outer) and southern hotspots derived from the unpublished 40"x80", 843 MHz MOST map of Dr. C.R. Subrahmanya and the present 1.4 GHz VLA map (smoothed to the same resolution), we calculated their ages as $4.5.10^7$ yr and $7.1.10^7$ yr. These imply average velocities of advance as 0.07c and 0.08c for the two hotspots respectively. The ages were calculated using the expression given by Willis and Strom (1978) for synchrotron aging :-

$$\alpha_{\nu_{\ell}}^{\nu_u} = \alpha_i - \frac{\gamma_i - 2}{Ln(\nu_u/\nu_{\ell})} \; Ln \left\{ \frac{(1 - \mu H_T^2 E_{\ell} \, t)}{(1 - \mu H_T^2 E_u \, t)} \right\}$$

Where α_i = the injection spectral index
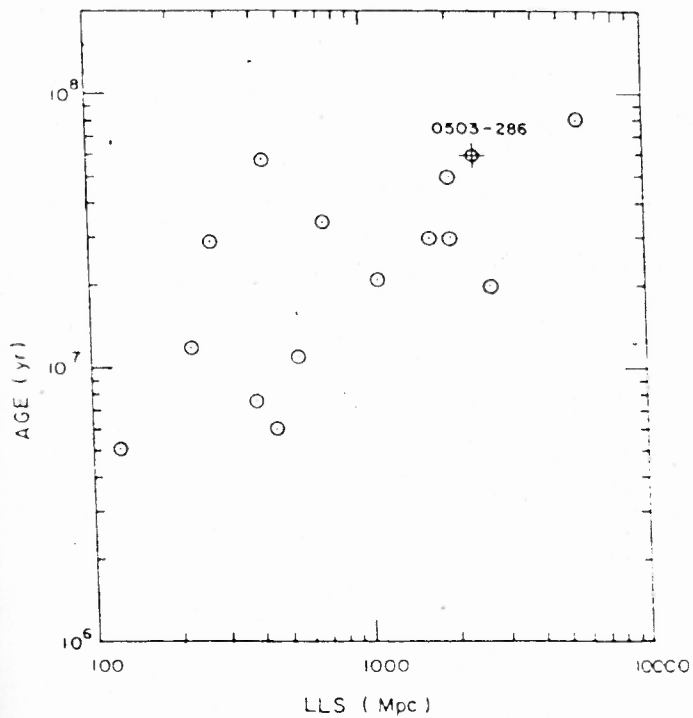
$\gamma_i = 2\alpha_i + 1$
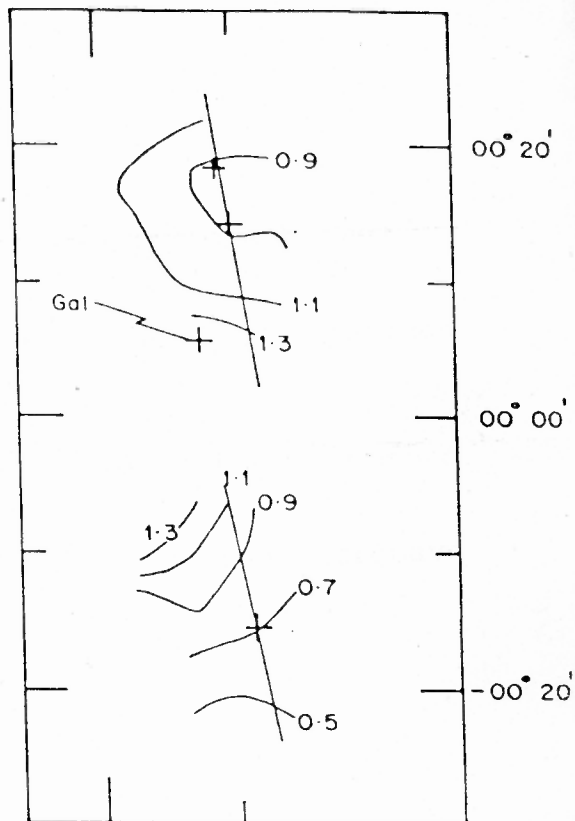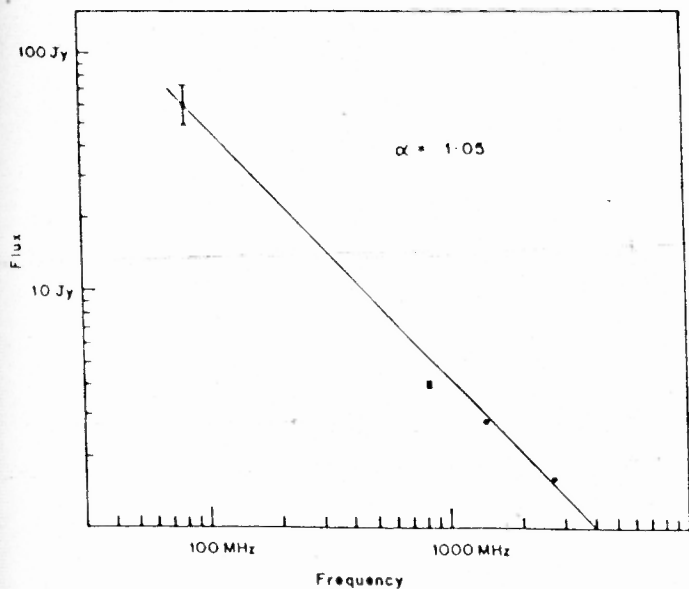
Fig.2.5 The integrated spectrum of 0503-286. The flux density values have been taken from the following sources: 85.5 MHz – Mills et al., 1960 (3.5 m cross); 843 MHz –Subrahmanya and Hunstead, 1986 (MOST); 1400 MHz and 2700 MHz –Saripalli et al., 1986 (100 m Effelsberg dish).

Fig.2.6 The 1.4 – 2.7 GHz spectral index distribution across 0503-286, using Effelsberg data with a 9'.3 arc resolution. The crosses indicate the emission peaks seen in Fig.2.1. The centre is at position $05^h03^m39^s-28^\circ45'00''$. The lines represent the long axes of the two lobes.

Fig.2.7 Plot of spectral age versus the largest linear size for a sample of FRII radio galaxies (see section 2.6). The GRG 0503-286 is shown with a cross.

$$\mu = 1.57 \times 10^{-3} \text{ cgs}$$

$\nu_u = $ higher frequency in Hz

$\nu_l = $ lower frequency in Hz

$\alpha = $ observed spectral index in the lobe between the lower (ν_1) and higher (ν_u) frequency

$t = $ time since particles were injected, in seconds

$H_T = [H^2 + H_{MBR}]^{1/2}$ in gauss

$H = $ equipartition magnetic field in the concerned region of the lobe

$H_{MBR} = $ equivalent magnetic field of the Microwave Background radiation

$$= 4.(1+z)^2 10^{-6} G$$

$$E_l = \left\{ \frac{\nu_l}{1.41.10^{18} H} \right\}^{1/2},$$

$$E_u = \left\{ \frac{\nu_u}{1.41.10^{18} H} \right\}^{1/2}$$

2.6   DISCUSSION

The radio structure of this source seen in Fig.2.1 and 2.2 and, in particular, the presence of only warmspots, is broadly consistent with its low radio power (Jenkins and McEllin, 1977). The source resembles the well known GRG NGC6251 in its marked lobe-core misalingment (Section 2.5) and the lobe asymmetry (defined as the ratio of the radio extents on either side of the parent galaxy). For comparing it with other GRGs, we list in Table 2.5 the observed properties of all 15 confirmed GRGs reported in the literature (Chapter I). The different columns are self-explanatory and the footnotes give additional relevant

Table 2.5 Comparison of the properties of giant radio sources

Name	Other Name	m	Morph class	Red shift	LAS	LLS	S^t_{408}	P^t_{408}	S^t_{5000}	ψ	D	Ref code	detection of jet	S^c_{5000}	β	Ref code
					arc	Mpc	Jy	10^{26}W/Hz	Jy	deg				Jy	"arc	
0055 +300	NGC 315	12.5pg	FR-II	0.0167	58	1.7	9.6	0.1	2.13	10	2.1	1,2	Yes	0.62	1 x 3	2
0114 -476		16.5R	FR-II	0.146	9.6	2.0	10.4	10.4	2.31	19	1.4	3,4	No	–	–	–
0136 +396	4C39.04	18R	FR-II	0.2107	7.3	2.0	3.3	8.0	0.24	2	1.2	5	No	0.011	4 x 6	10
0157 +405	4C40.08	16V	FR-I	0.078	14	1.7	4.9	1.5	0.39^b	0	1.2	6	No	0.005	3.7x5.8	6
0211 -479		17.6V	FR-II	0.22	5.6	1.6	3.4	8.5	0.42	2	1.7	7,8	No	–	–	–
0448 +519	3C130	16.5R	FR-I	0.1090	11.5	1.9	8.1	4.5	0.98	–	–	9	Yes	0.028	7 x 9	9
0503 -286		15R	FR-II	0.038	40	2.5	10.5	0.7	0.85	16	1.9	10	Yes	0.006	4	10
0744 +559	DA 240	15.2V	FR-II	0.0356	34	2.0	16.3	0.9	1.82	5	1.4	11,12	No	0.111	0.4	13
0945 +734	4C73.08	15.9p	FR-II	0.0581	18.5	1.7	10	1.5	0.89	1	1.5	14	Yes	0.011		10
1003 +351	3C236	16V	FR-II	0.0988	39	5.7	10.9	4.9	2.93	2	1.6	11,12	Yes	1.5	1 x 2	15
1331 -099		17.5R	FR-II	0.081	12.9	1.6	6.7	2.0	1.5^c	0	1.1	4,16	No	0.09	0.1	17
1452 -518		18J	FR-I/ II	(0.08)	20.3	2.5	4.7	1.5	2.1^d	10	1.8	18	Yes	0.135	25	18
1549 +202	3C326	15R	FR-II	0.0895	19.5	2.7	10.6	4.0	1.2	3	2.0	19	No	0.013	7 x 20	19
1637 +826	NGC6251	14B	FR-II	0.023	52	2.0	5.5	0.1	1.46	16	2.5	20,21 22	Yes	0.9	1	21
1721 +343	4C34.47	15.6V	FR-II	0.2055	7.3	1.8	3.1	2.0	0.8	0	1.1	23	Yes	0.44	6 x 10	23

[a] Computed for $H_O = 50$ km s^{-1} Mpc^{-1} and $q_o = 0$

[b] Extrapolated from 1.4GHz, using given, $\alpha = 1.01$

[c] Extrapolated from 408 MHz, assuming $\alpha = 0.6$

[d] Extrapolated from 1.4 GHz using derived $\alpha = 0.34$

ψ : Misalignment angle, defined as the supplement of the angle subtended at the core by the outermost peaks.

D : Ratio of the radio lobe extents.

β : HPBW of the beam corresponding to the map used in deriving S_{5000}.

Reference Codes: (1)Willis et al.,(1981); (2)Bridle et al.,(1979); (3)Danziger et al.,(1983); (4)Bolton et al.,(1964); (5)Hine (1979); (6)Faulkner,(1986); (7)Danziger et al.,(1978); (8)White et al.,(1984); (9)van Breugel et al.,(1986); (10)Present work; (11)Willis et al.,(1974); (12)Strom et al.,(1981); (13)van Breugel et al.,(1983); (14)Jägers (1986); (15)Fomalont et al.,(1979); (16)Schlizzi and McAdam (1975); (17)Graham et al.,(1981); (18)Jones, (1986); (19)Willis and Strom (1978); (20)Waggett et al.,(1977); (21)Jones et al.,(1986); (22)Willis et al.,(1982); (23)Jägers et al.,(1982);.

information. This compilation will be frequently used in subsequent chapters.

From Fig.2.2, the jet/counter-jet brightness ratio for this source is ~ 4 at 1.4 GHz. It has been established for radio galaxies that the jet prominence decreases with increasing total radio power (Bridle, 1986). This is consistent with the idea of a more efficient energy transportation in more powerful sources. In the classic example of the powerful radio galaxy, Cyg A, the jet accounts for only $\sim 0.25\%$ of the total emission at 1.4 GHz (Bridle, 1986). For the lower power (giant) radio galaxy NGC 6251, however, the jet-fraction is as high as 50% at 1.4 GHz (Waggett et al., 1977), with a similar value found for another low power giant radio galaxy, NGC315 (Willis et al., 1981). It is therefore surprising that despite its low radio power, $(P_{408} = 7.10^{25}$ WHz$^{-1})$ as well as the lack of bright hotspots (which are indicative of collimated, high Mach number jets in the beam model), 0503-286 has a low jet-fraction of only $\sim 0.3\%$ at 1.4 GHz. Another source in our sample of GRGs with a similar anomaly is DA240. However this GRG possesses one of the most compact hotspots, supporting the existence of a highly collimated, high Mach number jet, with an expected higher efficiency of energy transport. Also its radio power is relatively higher $(P_{408} \sim 9.10^{25}$ WHz$^{-1})$.

If jet emission is likely to be a result of dissipation in the energy transport, one would expect jets propagating through a denser medium to become intrinsically, brighter

(Bicknell, 1985; also, Scheuer,1987), as is thought to be the case for FRI type sources. As described in Section 2.4. an examination of the optical field of this source revealed a clear asymmetry in the distribution of galaxies within 2 magnitudes of the parent galaxy (Fig.2.4). This correlates interestingly with the marked asymmetry of the extents and powers of the two radio lobes (Chapter V). These correlations support the idea that both asymmetries are caused by the faster decceleration of the jet due to the higher density of the gas associated with the apparently stronger grouping of galaxies in the north (Saripalli et al., 1986). Under such conditions, it is therefore surprising that the detected jet is not to the north of the parent galaxy but to its south, where the ambient medium is expected to be less dense.

The peculiarities pointed out above in conjuction with the minimal projection effects expected for such a giant source considerably strain the twin-beam scenario for this jet. Within the flip-flop picture (Rudnick and Edgar, 1981) it is conceivable that the jet is currently active only in the southern lobe. Further, the abrupt termination of the jet suggests that it may be a newly forming jet. A minimum in the activity of the central engine in the recent past would also be consistent with the lack of bright hotspots in both lobes. However, more sensitive observations for the source are required for confirming the absence of a jet in the northern lobe. Redshift measurements for more galaxies seen in the north are required to establish physical association

among them, and with the radio galaxy. At present, redshift is available only for the spiral galaxy 'b', which is identical to that of radio galaxy 'a' (Fig.2.1; Saripalli et al., 1986).

The jet is seen to have many bright knots, and a prominent wiggle. It is separated from the core by an emission gap of ~ 13 kpc. This is similar to the gaps seen at the bases of the (detectable) jets in the powerful radio galaxies 3C219 (19.5 kpc), 3C388 (10.5kpc) and 3C438 (19.5 kpc), (Perley etal, 1984). Lower power radio galaxies like NGC 315, NGC6251 3C31 and 3C449 on the other hand, typically have considerably smaller, emission gaps. This is another anomaly noted for this source.

The large misalingment of the long axis of the northern lobe from the line joining the core to the outer warmspot is a further peculiarity of this source (Fig.2.1). The clustering of galaxies seen to the east (Fig.2.4) suggests an interesting evolutionary scenario to be put forward for this lobe. In this picture, both beams are ejected from the nucleus along the same axis in opposite directions, but the northern beam, has to propagate through a relatively denser intergalactic medium associated with the "cluster", which would slow its advance. Further, in this medium a large-scale decrease of gas density (and presumably of pressure too) from east to west can be inferred from the apparent distribution of the galaxies, as mentioned above. The trajectory of the beam may then be bent towards west, along

the pressure gradient (eg., Henriksen et al., 1981; Kundt and Gopal-Krishna, 1981). Also, the radio lobe formed around this northern beam, if filled with lighter than ambient material, would be subjected to buoyancy and thus be drifting westward in the direction of lower ambient density. Since such a drift is expected to be subsonic, the velocity should be $<10^3 kms^{-1}$ for a typical intra-cluster gas temperature of order $10^7 K$. Such a drift velocity, in conjunction with the actually observed physical offset of the lobe from the nucleus, which amounts to 3-4 arcmin ($\sim$ 200kpc;Fig.1b) would suggest a minimum age of $10^8 yr$ for this giant radio galaxy. The mean spectral age derived in Section 2.5 for this GRG 0503-286 is $\sim 6.10^7$ yr, similar to the spectral ages estimated for many other GRGs (DA240 and 3C236: $5.10^7 yr$, Strom et al., 1981; 4C73.08: $3.10^7 yr$, Mayer 1979; NGC6251 : 3.10^7, Waggett et al; 1977). The estimated spectral age of 0503-286 is thus quite similar to the minimum age of $\sim 10^8 yr$ derived from the scenario of the buoyantly drifting northern lobe. The estimate of age is seen to be consistent with the linear size vs spectral age trend found for FRII radio sources, in the sample studied by Alexander and Leahy (1987) (see Fig.2.7). We have also included 5 GRGs whose spectral ages are known (see above).

Studies pertaining to the radio core-fraction and the optical class of the GRG 0503-286 are described in detail in Chapter IV.

2.7 CONCLUSIONS

The radio/optical observations presented in this chapter have revealed several interesting properties associated with the 2.5 Mpc size GRG 0503-286, discovered by us. The pronounced asymmetry in the extents of the lobes on the two sides and the noticeable misalingment of the long axis of the northern lobe with respect to the line joining its outer peak with the nucleus could be explained in terms of a large-scale gradients in gas density, inferred from the relatively higher galaxy concentration seen to the north and east of the radio lobe. The discovery of a radio only jet to the south of the parent galaxy is not readily reconciliable with the observed asymmetry in the galaxy distribution around the source, prompting us to consider the alternate-ejection scenario. An age of $\sim 7.10^7$ yr is inferred for the source from the observed spectral gradients along the lobes. This is in close agreement with the age of $\sim 10^8$ yr derived from the buoyant drift scenario proposed for the northern lobe for explaining its large misalignment from the overall radio axis.